

Object as Query: Equipping Any 2D Object Detector with 3D Detection Ability

Zitian Wang¹ Zehao Huang² Jiahui Fu¹ Naiyan Wang² Si Liu¹

¹Institute of Artificial Intelligence, Beihang University

²TuSimple

{wangzt.kghl, zehaohuang18, winsty}@gmail.com {jiahui fu, liusi}@buaa.edu.cn

Abstract

3D object detection from multi-view images has drawn much attention over the past few years. Existing methods mainly establish 3D representations from multi-view images and adopt a dense detection head for object detection, or employ object queries distributed in 3D space to localize objects. In this paper, we design Multi-View 2D Objects guided 3D Object Detector (MV2D), which can be equipped with any 2D object detector to promote multi-view 3D object detection. Since 2D detections can provide valuable priors for object existence, MV2D exploits 2D detector to generate object queries conditioned on the rich image semantics. These dynamically generated queries enable MV2D to detect objects in larger 3D space without increased computational cost and show a strong capability of localizing 3D objects. For the generated queries, we design a sparse cross attention module to force them to focus on the features of specific objects, which reduces the computational cost and suppresses interference from noises. The evaluation results on the nuScenes dataset demonstrate the dynamic object queries and sparse feature aggregation do not harm 3D detection capability. MV2D also exhibits a state-of-the-art performance among existing methods. We hope MV2D can serve as a new baseline for future research.

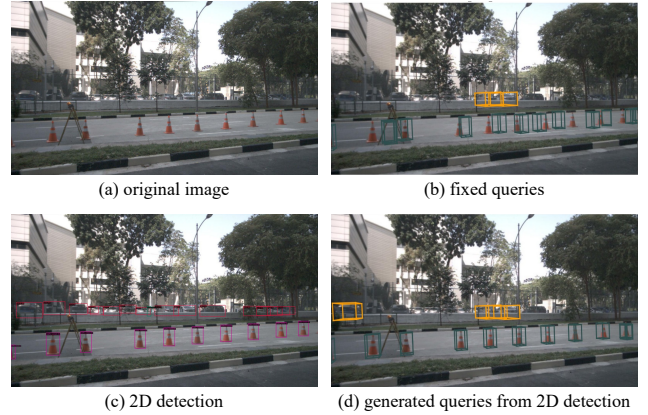


Figure 1. Motivation of MV2D. The 3D detector with fixed object queries (fixed queries means the queries are invariant for different inputs) might miss some objects, e.g., traffic cones (b), which are however successfully detected by a 2D detector (c). If generating object queries based on 2D detector, a 3D detector can produce more precise locations.

camera post-processing, which further causes degraded efficiency and efficacy. To handle these problems, recent researchers [14, 19, 20, 24, 39] propose to directly localize objects in 3D world space based on multi-view images, providing a new paradigm for vision-based 3D object detection.

1. Introduction

Camera-based 3D object detection in unconstrained real-world scenes has drawn much attention over the past few years. Early monocular 3D object detection methods [1, 15, 27, 33, 37, 38, 42] typically build their framework following the 2D object detection pipeline. The 3D location and attributes of objects are directly predicted from a single view image. Though these methods have achieved great progress, they are incapable of utilizing the geometric configuration of surrounding cameras and multi-view image correspondences, which are pivotal for the 3D position of objects in the real world. Moreover, adapting these methods to the multi-view setting relies on sophisticated cross-

According to the representation of fused features, current multi-view 3D object detection methods can be mainly divided into two streams: dense 3D methods and sparse query methods. Concretely, dense 3D methods render multi-view features into 3D space, such as Bird’s-Eye-View (BEV) feature space [4, 14, 19, 20] or voxel feature space [18, 32]. However, since the computational costs are squarely proportional to the range of 3D space, they inevitably cannot scale up to large-scale scenarios [7]. Alternatively, query-based methods [24, 39] adopt learnable object queries to aggregate features from multi-view images and predict object bounding boxes based on query features. Although fixed number of object queries avoid computational cost exploding with 3D space, the query number and position relied on

empirical prior may cause false positive or undetected objects in dynamic scenarios.

In this paper, we seek a more reliable way to generate object queries dynamically. The motivation comes from the rapid developments of 2D object detection methods [10, 21, 31, 34] which can generate high quality 2D bounding boxes for object localization in image space. Fortunately, 3D detectors are usually built upon 2D detection backbones. One natural idea is to turn each 2D detection into one query for the following 3D detection task. In this way, we design Multi-View 2D Objects guided 3D Object Detector (MV2D), which *could equip any 2D detector with 3D detection ability, and the 3D detector could harvest all the advancements from 2D detection field.*

Given the input multi-view images, we first obtain 2D detection results from a 2D detector and then generate a dynamic object query for each 2D bounding box. Instead of aggregating features from all regions in the multi-view inputs, one object query is forced to focus on one specific object. To this end, we propose an efficient correlated feature selection method based on the 2D detection results and camera configurations. Then the dynamically generated object queries, together with their 3D position embedded correlated features, are input to a transformer decoder with sparse cross-attention layers. Lastly, the updated object queries predict the final 3D bounding boxes.

Thanks to the powerful 2D detection performances, the dynamic queries generated from 2D detection results can cover most objects that appeared in the images, leading to higher precision and recall, especially for small and distant objects compared with fixed queries. As shown in Figure 1, the objects that a fixed query-based 3D detector might miss can be recalled in MV2D with the help of a 2D object detector. Theoretically, since 3D object queries stem from 2D detection results, our method can benefit from all off-the-shelf excellent 2D detector improvements. Our contributions can be summarized as:

- We propose a framework named MV2D that can be equipped with any 2D object detector to promote multi-view 3D object detection. Specifically, MV2D generates sparse dynamic object queries based on the results of 2D object detector.
- We demonstrate that sparse dynamic object queries and sparse aggregation from certain relevant regions in multi-view images do not sacrifice any detection performance.
- We test MV2D on the standard nuScenes dataset, and it achieves state-of-the-art performance among single frame methods.

2. Related Work

2.1. 2D Object Detection

2D object detection aims to predict and localize objects in 2D images, which is a fundamental problem in computer vision. The RCNN series [9, 10, 21, 31] propose a two-stage pipeline for 2D object detection. These methods first generate a set of region proposals likely to contain objects in the image, then make a second stage decision on the object classification and bounding box regression. Another group of researchers investigate to detect object in a single-stage pipeline [22, 30, 34], aiming to provide faster detectors for deployment. Recently, DETR [3] introduces a transformer encoder-decoder architecture into 2D object detection and formulates object detection as a set prediction problem. In DETR, a set of learnable object queries are adopted to interact with image features and responsible for detection objects. Deformable DETR [44] improves DETR by introducing multi-scale deformable attention. Besides, it transfers the vanilla DETR into a two-stage framework, where region proposals are firstly generated based on encoder features and then sent to the decoder as object queries for further refinement.

2.2. Vision-based 3D Object Detection

The goal of vision-based 3D object detection is to predict 3D bounding boxes from camera images. Many previous [1, 15, 28, 33, 37, 38] works perform this task based on the single-view image setting. Concretely, these methods mostly focus on instance depth estimation and use an extra depth prediction module to complement 2D detectors on depth information. However, when dealing with multi-view images surrounding the ego vehicle, these methods need to detect objects from each view and project them to the same 3D space with cumbersome NMS post-processing to merge results.

Recently, some works attempt to directly detect objects in 3D space from multi-view images. One branch of these methods lift 2D image into 3D space, then conduct detection based on the 3D representations. ImVoxelNet [32] builds a 3D voxelized space and samples image features from multi-view to obtain the voxel representation. BEVFormer [20] leverages dense BEV queries to project and aggregate features from multi-view images by deformable attention [44]. BEVDet and BEVDepth [14, 19] adopt the Lift-Splat module [29] to transform multi-view image features into the BEV representation based on the predicted depth distribution. Although such 3D space representations are conducive to unifying multi-view images, the memory consumption and computational cost would increase rapidly with the enlarging of the detection range in 3D space.

Another way of such works adopts learnable object queries to aggregate image features and predict objects fol-

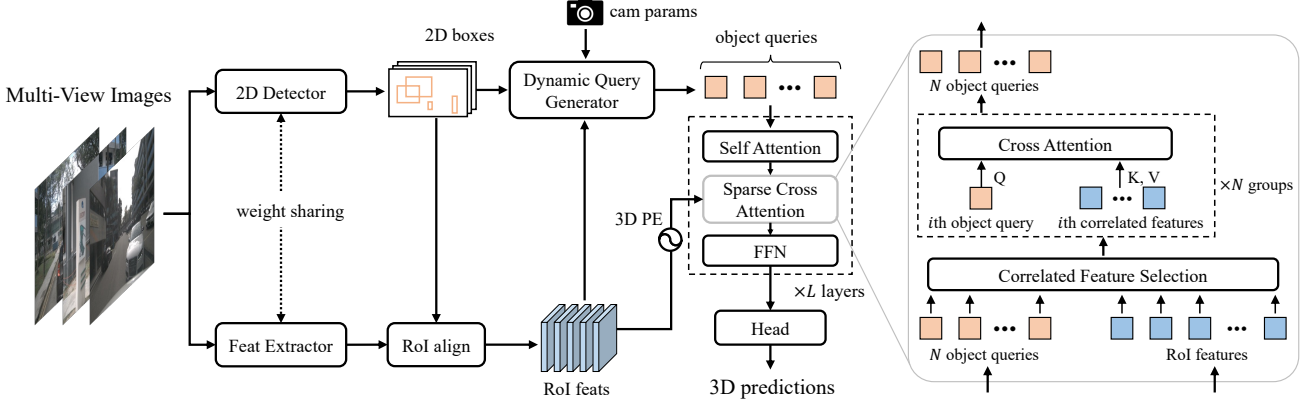


Figure 2. The framework of the proposed MV2D. Given the input multi-view images, a 2D detector is used to obtain per-view 2D detection results. Meanwhile, image feature maps are extracted by a feature extractor. The parameter weights of the backbone network of 2D detector and feature extractor can be shared. Then the RoI features are extracted through RoI-align for detected 2D bounding boxes. Based on the RoI features, RoI positions and camera parameters, MV2D initializes a set of object queries using a dynamic query generator. These generated object queries and RoI features with 3D PE (3D position embedding) [24] are input to a decoder to update query features. Compared to vanilla transformer decoder, the decoder in MV2D employ sparse cross attention where each object query only interact with its correlated features. Lastly, a prediction head is applied on the updated object queries to generate 3D detection results.

lowing the DETR [3] framework. DETR3D [39] generates 3D reference points from object queries and projects them to multi-camera images by camera parameters. Then the query features are refined by the corresponding point features sampling from images. In contrast to establishing fixed mapping through 3D-to-2D query projecting, some methods learn the flexible mapping via attention mechanisms [24, 41]. PETR [24] introduces 3D position-aware image features and learns the flexible mapping between query and image features by global cross-attention. Nonetheless, these approaches usually require dense object queries distributed in 3D space to ensure sufficient recall of objects.

In this paper, we propose a 2D objects guided framework for multi-view 3D object detection. Based on the 2D detector, our method can count on much sparser queries to recall the objects and eliminate the interference of noises and distractors.

3. Method

3.1. Overview

The overall pipeline of MV2D is shown in Figure 2. Given N multi-view images $\mathcal{I} = \{\mathbf{I}_v \mid 0 \leq v < N\}$, image feature maps $\mathcal{F} = \{\mathbf{F}_v \mid 0 \leq v < N\}$ are first extracted from the input images using a backbone network, where $\mathbf{F}_v \in \mathbb{R}^{H^f \times W^f \times C}$ is the extracted feature map from the v -th image. To get 2D object detection, a 2D object detector, i.e., Faster R-CNN [31], is applied to all the input images, resulting in a set of 2D object bounding boxes $\mathcal{B} = \{\mathbf{B}_v \mid 0 \leq v < N\}$, where $\mathbf{B}_v \in \mathbb{R}^{M_v \times 4}$ represents the predicted 2D bounding boxes in the v -th image and M_v

is the number of detected boxes. In practice, the weights of the backbone of 2D detector can also be used for subsequent feature extraction.

Different from common methods in multi-view 3D object detection which adopt fixed object queries across the whole dataset [24, 39], MV2D generates object queries conditioned on the input multi-view images. Given the predicted 2D bounding boxes and extracted image features, MV2D employs RoI-Align [11] to extract 2D object features. Then the 2D object features together with corresponding bounding boxes and camera parameters are input to the dynamic object query generator to produce object queries. For each object query, relevant image features in multi-view images are selected based on 2D detection results and camera parameters through a feature selection module. Then the object queries interact with each other and integrate information from correlated object features iteratively through transformer decoder layers [35]. Finally, a simple feed forward network (FFN) head is used to generate 3D object predictions with updated features.

3.2. Dynamic Object Query Generation

With the help of an effective 2D object detector, the object existences are well demonstrated and the object locations are constrained within certain image regions, thus providing valuable priors for localizing objects in 3D space.

To generate object queries from 2D detection results, we propose a dynamic query generator as shown in Figure 3. The dynamic query generator derives a 3D reference point $\mathbf{p}_{ref} \in \mathbb{R}^3$ in 3D world space for each RoI. Then the object query is generated from \mathbf{p}_{ref} by a positional encoding layer [35].

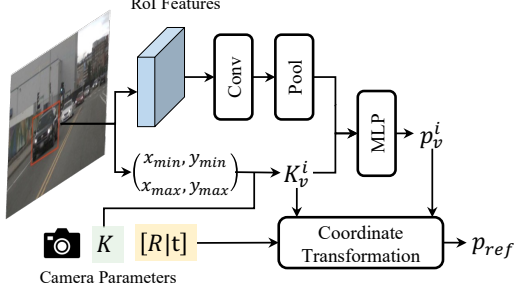


Figure 3. Dynamic object query generator.

Specifically, given the 2D object detection results \mathcal{B} and image feature maps \mathcal{F} from all the images, we first extract object RoI features \mathcal{O} through RoI-Align, where $\mathbf{O}_v \in \mathbb{R}^{M_v \times H^{roi} \times W^{roi} \times C}$ are the RoI features corresponding to 2D object bounding boxes \mathbf{B}_v :

$$\mathbf{O}_v = \text{RoI-Align}(\mathbf{F}_v, \mathbf{B}_v), \quad 0 \leq v < N. \quad (1)$$

The RoI features \mathbf{O}_v contain sufficient object appearance information to infer the object center locations in image space. However, further estimating the object depths directly from RoI features is difficult. As the object region in original image space is rescaling into a fixed sized RoI, the geometric information contained in original images are missed.

Taking this into consideration, we apply equivalent camera intrinsic transformation to each RoI, such that the rescaling operation conducted on different RoIs is equivalent to perspective projection with different camera parameters. Thus a point in the RoI coordinate system can be transformed to 3D world space with equivalent camera intrinsic:

$$\mathbf{p}_{3d} = [\mathbf{R}|\mathbf{t}]^{-1}(\mathbf{K}_{roi})^{-1} \mathbf{p}_{roi}, \quad (2)$$

where $\mathbf{p}_{roi} \in \mathbb{R}^4$ (homogeneous coordinate) represents the point in RoI coordinate system, $\mathbf{p}_{3d} \in \mathbb{R}^4$ represents the point in 3D world space, \mathbf{K}_{roi} is the equivalent camera intrinsic of that RoI and $[\mathbf{R}|\mathbf{t}]$ is the camera extrinsic.

Denote the RoI size is $H^{roi} \times W^{roi}$ (e.g., 7×7), the i -th 2D object bounding box in the v -th view is $\mathbf{B}_v^i = (x_{min}^i, y_{min}^i, x_{max}^i, y_{max}^i)$, and the original camera intrinsic matrix is:

$$\mathbf{K}_v = \begin{bmatrix} f_x & 0 & o_x & 0 \\ 0 & f_y & o_y & 0 \\ 0 & 0 & 1 & 0 \\ 0 & 0 & 0 & 1 \end{bmatrix}. \quad (3)$$

The equivalent camera intrinsic for i -th RoI can be formulated as:

$$\mathbf{K}_v^i = \begin{bmatrix} f_x * r_x & 0 & (o_x - x_{min}^i) * r_x & 0 \\ 0 & f_y * r_y & (o_y - y_{min}^i) * r_y & 0 \\ 0 & 0 & 1 & 0 \\ 0 & 0 & 0 & 1 \end{bmatrix}, \quad (4)$$

where $r_x = W^{roi}/(x_{max}^i - x_{min}^i)$, $r_y = H^{roi}/(y_{max}^i - y_{min}^i)$.

Since the equivalent camera intrinsic matrix contains the geometric property of the camera and object, we adopt a small network to implicitly encode the object location $\mathbf{p}_v^i \in \mathbb{R}^4$ based on the RoI feature \mathbf{o}_v^i and the equivalent camera intrinsic \mathbf{K}_v^i :

$$\mathbf{p}_v^i = \mathcal{H}(\text{MLP}(\text{Pool}(\text{Conv}(\mathbf{o}_v^i)); \mathbf{K}_v^i)), \quad (5)$$

where $(;)$ means feature concatenation and $\mathcal{H}(\cdot)$ represents homogeneous transformation.

The implicitly encoded object location \mathbf{p}_v^i , which can be seen as the 3D object location in RoI coordinate system, is then transformed into 3D world space using equivalent camera intrinsic and camera extrinsic as in Equation 2. Consequently, the transformed 3D location serves as reference point \mathbf{p}_{ref} for localizing object in 3D world space.

By this transformation, MV2D generates a set of dynamic reference points $\mathcal{P}_{ref} = \{\mathbf{p}_{ref,v} \in \mathbb{R}^{M_v \times 3} \mid 0 \leq v < N\}$ based on 2D detections and camera configurations. These reference points are then passed through a 3D positional encoding layer to initialize a set of object queries $\mathcal{Q} = \{\mathbf{Q}_v \in \mathbb{R}^{M_v \times C} \mid 0 \leq v < N\}$.

3.3. Relevant Object Feature Selection

Each object is only captured in a sub-region within the input multi-view images. To precisely depict a certain object, an object query should focus on all the relevant image regions that cover the target object, and discard irrelevant regions that might mislead the 3D localization of the target object.

To this end, we propose to select relevant features for each object query's updating. Since 2D object detector can predict convincing 2D object proposals, the detected object bounding boxes imply which region contains the most distinctive information about an object. So we consider two parts of the relevant features of an object: (1) the 2D bounding box \mathbf{b}_v^i from where the object query is generated; (2) the bounding boxes in other views that corresponds to \mathbf{b}_v^i .

In this paper, we develop an efficient method to associate the bounding boxes in other views for a given query. As shown in Figure 4, we create a 3D meshgrid $\mathbf{G} \in \mathbb{R}^{W^{roi} \times H^{roi} \times D \times 4}$ for each RoI. We denote $\mathbf{g}_{x,y,z} = (x \times d_z, y \times d_z, d_z, 1)$ as each point in the meshgrid, where (x, y) is the coordinate in the RoI, $d_z \in \{d_0, d_1, \dots, d_{D-1}\}$ is a set of predefined depth values. The meshgrid of RoI is then transformed into the coordinate system of the w -th view:

$$\mathbf{g}_{v \rightarrow w; x, y, z}^i = \mathbf{K}_w \mathbf{T}_{v \rightarrow w} (\mathbf{K}_v^i)^{-1} \mathbf{g}_{x, y, z}, \quad (6)$$

where $\mathbf{g}_{v \rightarrow w; x, y, z}^i$ is the transformed meshgrid point in the w -th view and $\mathbf{T}_{v \rightarrow w}$ is the coordinate transformation matrix from the v -th view to the w -th view.

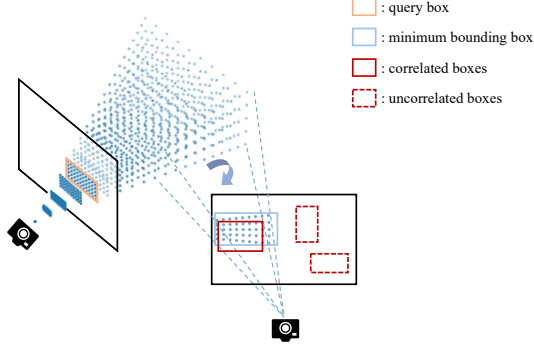


Figure 4. Illustration of relevant region selection. Each query box generates a discretized camera frustum from 3D meshgrid. The camera frustum is then projected to another view’s pixel coordinate to calculate a minimum bounding box. Then correlated box is selected based on IoU with the minimum bounding box.

According to the transformed meshgrid $\mathbf{G}_{v \rightarrow w}^i$, a minimum bounding box $\mathbf{b}_{v \rightarrow w}^i$ in the image space of the w -th view can be calculated. Then the detected box that has highest Intersection-over-Union (IoU) with $\mathbf{b}_{v \rightarrow w}^i$ (if greater than 0) is selected as correlated box in the w -th view:

$$\mathbf{b}_{corr, v \rightarrow w}^i = \arg \max_{\mathbf{b}_w^j \in \mathbf{B}_w} \text{IoU}(\mathbf{b}_{v \rightarrow w}^i, \mathbf{b}_w^j). \quad (7)$$

Then, only the RoI features of \mathbf{b}_v^i and $\{\mathbf{b}_{corr, v \rightarrow w}^i \mid 0 \leq w < N, w \neq v\}$ will be adopted to update object query \mathbf{q}_v^i . We will describe the details in the following section.

3.4. Decoder with Sparse Cross Attention

The generated object queries interact with their relevant features through a DETR-like transformer decoder [3, 24]. 3D position embedding is provided for the relevant features following PETR [24]. The difference in our decoder lies in the sparse cross attention layer as shown in Figure 2. Instead of using the whole multi-view feature maps to construct keys and values shared by all the queries, MV2D only uses the relevant features to construct their own keys and values for each object query. This design not only contributes a compact set of keys and values, but also prevents the object queries from being interfered by background noises and distractors.

Lastly, we apply classification head and regression head composed of MLPs to the updated object queries to predict the final 3D object detection results.

3.5. Loss Functions

In our implementation, the 2D detector and the 3D detector are jointly trained in MV2D, with the backbone weights shared across both detectors. The 2D object detection loss \mathcal{L}_{2d} is directly taken from 2D detectors. As for 3D object detection loss, we follow previous works [24, 39] to

use Hungarian algorithm [16] for label assignment. Focal loss [22] and L_1 loss are adopted for classification and box regression respectively. The 3D object detection loss can be summarized as:

$$\mathcal{L}_{3d} = \lambda_{cls3d} \cdot \mathcal{L}_{cls3d} + \mathcal{L}_{reg3d}. \quad (8)$$

The overall loss function of MV2D is:

$$\mathcal{L} = \mathcal{L}_{2d} + \lambda_{3d} \cdot \mathcal{L}_{3d}, \quad (9)$$

where λ_{3d} is the weight term to balance 2D detection and 3D detection losses, set to 0.1 in our experiments.

4. Experiments

4.1. Datasets and Metrics

We validate the effectiveness of MV2D on the large-scale nuScenes dataset [2]. NuScenes contains 1000 driving sequences, which are divided into 700 samples for training, 150 samples for validation, and 150 samples for testing, respectively. Each sequence is approximately 20-second long, including annotated 3D bounding boxes from 10 categories of sampled key frames. Each sample consists of 6 surround-view images with 1600×900 resolution, which provide 360° horizontal FOV in total. We submit *test* set results to the online server for official evaluation. Other experiments are based on the *val* set.

4.2. Implementation Details

Training and evaluation All the models are trained using AdamW [26] optimizer with a weight decay of 0.01. Cosine annealing policy [25] is adopted and the initial learning rate is set to 2×10^{-4} . Since MV2D generates object queries from 2D detection results, we pretrain the 2D detectors on nuImages [2] to provide appropriate initialization. Since nuScenes dataset does not provide 2D bounding box annotations, we generate the box labels from 3D bounding boxes following [40]. We employ image-space augmentation (e.g., random flip, crop and resize) and BEV-space augmentation [14] during training. If not specified, the models are trained for 24 epochs without CBGS [43]. No test time augmentation is used during inference. Our implementation is based on MMDetection3D [5].

Network architecture Faster-RCNN [31] is adopted as 2D detector in our experiments. The 2D score threshold and Non-maximum Suppression (NMS) IoU threshold are set to 0.05 and 0.6 respectively. We use ResNet-50, ResNet-101 [12] and VoVNetV2 [17] as backbone networks. ResNet-50 and ResNet-101 are equipped with deformable convolution [6] in the 3rd and 4th stages. VoVNetV2 is initialized from a DD3D checkpoint trained with extra data [28]. RoI-align is applied on the P4 stage of

Method	Backbone	Resolution	NDS \uparrow	mAP \uparrow	mATE \downarrow	mASE \downarrow	mAOE \downarrow	mAVE \downarrow	mAAE \downarrow
DETR3D [39]	Res-50	1600 \times 900	0.373	0.302	0.811	0.282	0.493	0.979	0.212
BEVDepth* [19]	Res-50	704 \times 256	0.367	0.315	0.702	0.271	0.621	1.042	0.315
PETR [24]	Res-50	1408 \times 512	0.403	0.339	0.748	0.273	0.539	0.907	0.203
MV2D \ddagger	Res-50	1408 \times 512	0.433	0.388	0.697	0.271	0.479	0.952	0.208
FCOS3D \dagger [37]	Res-101	1600 \times 900	0.415	0.343	0.725	0.263	0.422	1.292	0.153
PGD \dagger [38]	Res-101	1600 \times 900	0.428	0.369	0.683	0.260	0.439	1.268	0.185
DETR3D \dagger [39]	Res-101	1600 \times 900	0.425	0.346	0.773	0.268	0.383	0.842	0.216
BEVDepth* [19]	Res-101	1408 \times 512	0.408	0.376	0.659	0.267	0.543	1.059	0.335
BEVFormer-S \dagger [20]	Res-101	1600 \times 900	0.448	0.375	0.725	0.272	0.391	0.802	0.200
PETR \dagger [24]	Res-101	1600 \times 900	0.442	0.370	0.711	0.267	0.383	0.865	0.201
MV2D \ddagger	Res-101	1600 \times 900	0.451	0.406	0.685	0.265	0.446	0.912	0.215

Table 1. **3D object detection results on nuScenes val set.** \dagger : the model is initialized from a FCOS3D backbone. \ddagger : the model is pretrained on nuImages. *: the model uses extra modal data (e.g., point clouds) during training.

Method	Backbone	NDS \uparrow	mAP \uparrow	mATE \downarrow	mASE \downarrow	mAOE \downarrow	mAVE \downarrow	mAAE \downarrow
FCOS3D \dagger [37]	Res-101	0.428	0.358	0.690	0.249	0.452	1.434	0.124
PGD \dagger [38]	Res-101	0.448	0.386	0.626	0.245	0.451	1.509	0.127
BEVFormer-S \dagger [20]	Res-101	0.462	0.409	0.650	0.261	0.439	0.925	0.147
PETR \dagger [24]	Res-101	0.455	0.391	0.647	0.251	0.433	0.933	0.143
MV2D \ddagger	Res-101	0.462	0.427	0.640	0.257	0.457	0.997	0.162
BEVDet [14]	Swin-Base	0.488	0.424	0.524	0.242	0.373	0.950	0.148
M2BEV [40] \ddagger	ResNeXt-101	0.474	0.429	0.583	0.254	0.376	1.053	0.190
DETR3D \S [39]	V2-99	0.479	0.412	0.641	0.255	0.394	0.845	0.133
BEVFormer-S \S [20]	V2-99	0.495	0.435	0.589	0.254	0.402	0.842	0.131
PETR \S [24]	V2-99	0.504	0.441	0.593	0.249	0.383	0.808	0.132
MV2D $\S\ddagger$	V2-99	0.514	0.463	0.542	0.247	0.403	0.857	0.127

Table 2. **3D detection results on nuScenes test set.** \dagger : the model is initialized from a FCOS3D checkpoint. \ddagger : the model is pretrained on nuImages. \S : the model is initialized from a DD3D [28] checkpoint trained with external data.

FPN [21] with RoI size 7×7 for dynamic object query generation and correlated feature selection. The decoder contains 6 transformer decoder layers, followed by MLP head to produce classification and regression results.

4.3. Comparison with State-of-the-arts

We compare the MV2D performance with state-of-the-art methods on nuScenes *val* set and *test* set under *single frame setting*. The results are shown in Table 1 and Table 2.

Table 1 shows comparison on nuScenes *val* set. From the table, MV2D achieves higher performance with both ResNet-50 and ResNet-101 backbone, especially on mAP. The significant improvement on mAP suggests MV2D has a strong capability at localizing objects in 3D space. In comparison with multi-view 3D object detection methods, MV2D with ResNet-101 outperforms BEV based methods BEVFormer-S [20] by 3.1% and 0.3% on mAP and NDS, and outperforms BEVDepth [19] with extra depth supervision by 3.0% and 4.3% on mAP and NDS. In comparison with query

based methods, MV2D outperforms the best performing PETR [24] by 3.6% and 0.9% on mAP and NDS.

Table 2 shows the comparison on nuScenes *test* set. We use both the training and validation splits for training MV2D. As can be seen from the table, MV2D with ResNet-101 backbone achieves 42.7% mAP and 46.2% NDS, which outperforms existing methods by 1.8% on mAP. For MV2D with VoVNetV2, we train it for 90 epochs without CBGS (which has almost the same amount of samples as training 24 epochs with CBGS) for better performance. In that case, MV2D achieves 46.3% mAP and 51.4% NDS, which improves mAP by 2.2% compared to PETR. Note that our method gets larger mAVE compared to state-of-the-arts, which is the main cause of degraded NDS.

4.4. Ablation Study

In this section, we provide a detailed analysis on the core design choices of MV2D. All the experiments are based on ResNet-50 backbone. For fair comparison, we design a

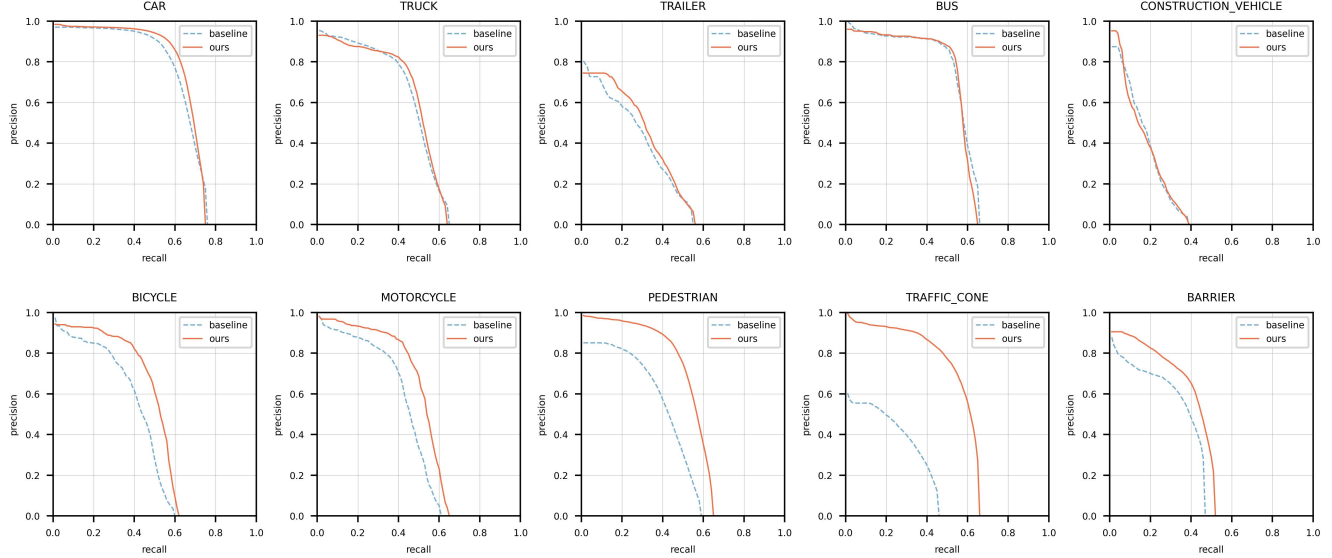


Figure 5. Precision-recall curves of different classes under a 2D object detection setting. The models still produce 3D object predictions, while the 2D bounding boxes in each image are generated by projecting 3D bounding boxes using camera parameters. Precision & recall are calculated with 2D IoU threshold 0.5 in nuScenes *val* set. The blue dash line represents the *baseline* method (fixed object queries). The red solid line represents our method (generated object queries).

#	object query	key & value	mAP \uparrow	NDS \uparrow
1	fixed ($\times 900$)	all feats	36.2	39.9
2	fixed ($\times 300$)	all feats	36.1	39.4
3	fixed ($\times 1500$)	all feats	36.6	40.6
4	generated ($\times 165$)	all feats	38.0	41.2
5	generated ($\times 165$)	all RoIs	37.9	41.1
6	generated ($\times 165$)	correlated RoIs	38.8	43.3

Table 3. Ablation study on the object query and key & value in the cross attention layers. The number of generated queries is calculated on average.

baseline method also trained with a 2D detector and initialized from a nuImages pretrained checkpoint. This method uses a fixed number of learnable object queries to aggregate information from the whole multi-view feature maps as in PETR [24]. As in Table 3, we denote the design in #1 which follows PETR to use 900 object queries as *baseline* in our experiments.

Generated object queries vs. fixed object queries We first compare the generated object queries with fixed object queries. From #1 to #3 in Table 3, it can be observed that in the case of fixed queries, a larger query amount can improve performance since the fixed query based methods rely on densely placed object queries to localize objects. However, the computational cost and memory consumption also rise with the growth of query density. According to #4, when replacing the fixed queries by dynamically generated queries, mAP and NDS are improved by 1.8% and 1.3%

#	2D NMS IoU	2D score thr	RoI size	mAP \uparrow	NDS \uparrow
1	0.5	0.05	7	38.2	42.9
2	0.6	0.05	7	38.8	43.3
3	0.7	0.05	7	37.4	41.1
4	0.6	0.1	7	38.5	43.2
5	0.6	0.2	7	38.0	42.9
6	0.6	0.05	14	38.6	43.1

Table 4. Ablation study on RoI configurations.

respectively. Note that the number of generated queries is only around 165 on average, which is much less than that of fixed queries. This demonstrates the object queries generated by 2D detector produce higher-quality object location hypotheses even with smaller query amount.

Effectiveness of correlated features We also validate the effectiveness of using only correlated features for object query updating. In Table 3, #4 represents using the whole multi-view feature maps for each object query, #5 represents using all the RoI features for each object query, while #6 represents using only the correlated RoI features for each object query. As shown by the results, simply replacing the whole feature maps by all RoI features does not bring performance gain. Nevertheless, using only the correlated RoI features for object query updating as introduced in Section 3.3 can improve mAP and NDS by 0.8% and 2.1% respectively. This result verifies the effectiveness of object query to aggregate information in a specified foreground region.

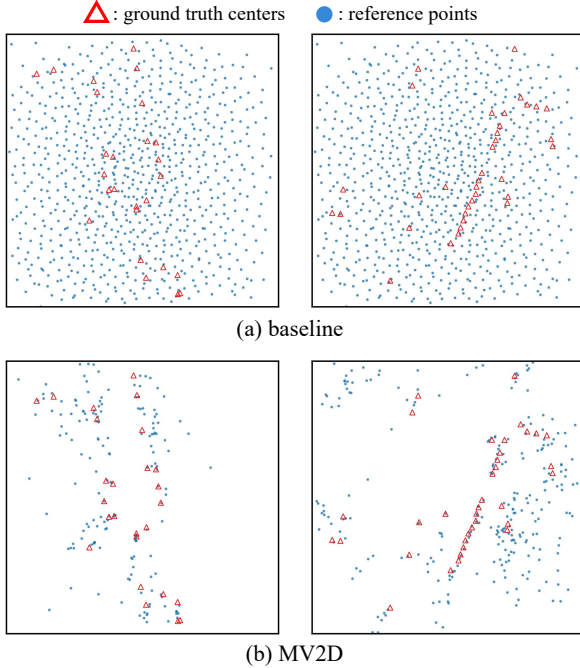


Figure 6. Illustration of different kinds of object queries. The top row (a) represents the *baseline* method (fixed object queries) and the bottom row (b) represents our method (generated object queries). We visualize ground truth center locations and the reference points in BEV space. The samples are taken from nuScenes val set. We suggest readers view this figure with zooming in.

Influence of RoI configuration In this part, we study the influence of different RoI configurations in MV2D. We experiment with different 2D detection score thresholds, 2D NMS IoU thresholds, and RoI-align sizes. The results are listed in Table 4. As can be seen from the table, the performance of MV2D is robust to different RoI settings.

4.5. Qualitative Analysis

In this section, we analyze how might a 2D detector promote the performance of multi-view 3D object detection. To verify if the object queries generated from 2D detector can better localize objects with the help of image semantics, we compare the 2D object detection performance of the *baseline* method (fixed object queries) and our method (generated object queries) by perspective projection. Specifically, we project the 3D bounding boxes into each image, then calculate the minimum 2D bounding boxes as 2D results. The performance is evaluated between the projected 2D bounding boxes of predictions and ground truths. We set the IoU threshold to 0.5 for true positive assignment.

In Figure 5, we draw the precision-recall curves of 10 classes in nuScenes. As seen from the figure, our method achieves higher precision and recall compared to the *baseline* method, especially for the classes with relatively smaller size. This demonstrates that 2D object detectors can make the most of image semantics to discover ob-

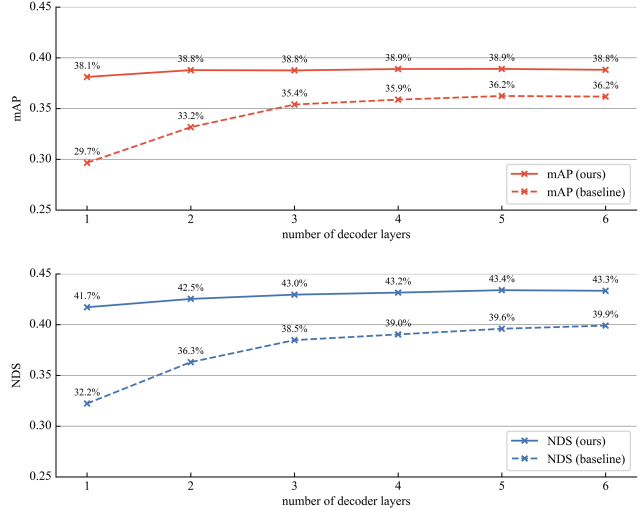


Figure 7. Comparison under different numbers of decoder layers.

jects from image space, which can serve as solid evidence of object existence to be exploited by 3D detectors. For complementary, we provide the visualization of different kinds of queries in Figure 6. Though the generated queries are much sparser compared to the fixed queries, they are mostly distributed around the objects.

Moreover, we compare the 3D detection performance of *baseline* and our method under different numbers of decoder layers. As shown in Figure 7, *baseline* with fixed queries rely on a heavy decoder to refine the query features. In contrast, our method with generated queries and sparse cross attention shows a faster convergence on mAP and NDS. This result demonstrates that better initialized queries and constrained search regions might help to reduce the ambiguity for localizing objects.

5. Conclusion

In this paper, we propose Multi-View 2D Objects guided 3D Object Detector (MV2D) for multi-view 3D object detection. In our framework, we utilizes 2D objects as sparse queries and adopt a sparse cross attention module to limit the attention region of queries. In our experiments, we demonstrate promising results on nuScenes dataset with our proposed sparse dynamic object queries and sparse aggregation strategies. Our framework can equip any 2D detector with 3D detection ability, and we believe the insight of utilizing the 2D objects as guidance can further inspire the design of multi-view 3D object detection methods.

Limitations Since MV2D generates object queries from 2D detections, an object might be missed if the 2D detector fails to recall it. Besides, it requires careful design of temporal correlation for MV2D under multi-frame setting. We look forward to further extending MV2D in the temporal dimension in the future.

References

- [1] Garrick Brazil and Xiaoming Liu. M3D-RPN: monocular 3d region proposal network for object detection. In *ICCV*, 2019. 1, 2
- [2] Holger Caesar, Varun Bankiti, Alex H. Lang, Sourabh Vora, Venice Erin Liong, Qiang Xu, Anush Krishnan, Yu Pan, Giancarlo Baldan, and Oscar Beijbom. nuscenes: A multi-modal dataset for autonomous driving. In *CVPR*, 2020. 5, 11
- [3] Nicolas Carion, Francisco Massa, Gabriel Synnaeve, Nicolas Usunier, Alexander Kirillov, and Sergey Zagoruyko. End-to-end object detection with transformers. In *ECCV*, 2020. 2, 3, 5
- [4] Shaoyu Chen, Xinggang Wang, Tianheng Cheng, Qian Zhang, Chang Huang, and Wenyu Liu. Polar parametrization for vision-based surround-view 3d detection. *arXiv preprint arXiv:2206.10965*, 2022. 1
- [5] MMDetection3D Contributors. MMDetection3D: Open-MMLab next-generation platform for general 3D object detection. <https://github.com/open-mmlab/mmdetection3d>, 2020. 5
- [6] Jifeng Dai, Haozhi Qi, Yuwen Xiong, Yi Li, Guodong Zhang, Han Hu, and Yichen Wei. Deformable convolutional networks. In *ICCV*, 2017. 5, 11
- [7] Lue Fan, Feng Wang, Naiyan Wang, and Zhaoxiang Zhang. Fully sparse 3d object detection. In *NeurIPS*, 2022. 1
- [8] Zheng Ge, Songtao Liu, Feng Wang, Zeming Li, and Jian Sun. YoloX: Exceeding yolo series in 2021. *arXiv preprint arXiv:2107.08430*, 2021. 11
- [9] Ross Girshick. Fast R-CNN. In *ICCV*, 2015. 2, 11
- [10] Ross Girshick, Jeff Donahue, Trevor Darrell, and Jitendra Malik. Rich feature hierarchies for accurate object detection and semantic segmentation. In *CVPR*, 2014. 2, 11
- [11] Kaiming He, Georgia Gkioxari, Piotr Dollár, and Ross Girshick. Mask R-CNN. In *ICCV*, 2017. 3, 11
- [12] Kaiming He, Xiangyu Zhang, Shaoqing Ren, and Jian Sun. Deep residual learning for image recognition. In *CVPR*, 2016. 5
- [13] Kaiming He, Xiangyu Zhang, Shaoqing Ren, and Jian Sun. Deep residual learning for image recognition. In *CVPR*, 2016. 11
- [14] Junjie Huang, Guan Huang, Zheng Zhu, and Dalong Du. BEVDet: High-performance multi-camera 3d object detection in bird-eye-view. *arXiv preprint arXiv:2112.11790*, 2021. 1, 2, 5, 6
- [15] Jason Ku, Alex D. Pon, and Steven L. Waslander. Monocular 3d object detection leveraging accurate proposals and shape reconstruction. In *CVPR*, 2019. 1, 2
- [16] Harold W Kuhn. The hungarian method for the assignment problem. *Naval research logistics quarterly*, 1955. 5
- [17] Youngwan Lee, Joong-Won Hwang, Sangrok Lee, Yuseok Bae, and Jongyoul Park. An energy and gpu-computation efficient backbone network for real-time object detection. In *CVPRW*, 2019. 5
- [18] Yanwei Li, Yilun Chen, Xiaojuan Qi, Zeming Li, Jian Sun, and Jiaya Jia. Unifying voxel-based representation with transformer for 3d object detection. In *NeurIPS*, 2022. 1
- [19] Yin hao Li, Zheng Ge, Guanyi Yu, Jinrong Yang, Zengran Wang, Yukang Shi, Jianjian Sun, and Zeming Li. BEVDepth: Acquisition of reliable depth for multi-view 3d object detection. *arXiv preprint arXiv:2206.10092*, 2022. 1, 2, 6
- [20] Zhiqi Li, Wenhai Wang, Hongyang Li, Enze Xie, Chonghao Sima, Tong Lu, Qiao Yu, and Jifeng Dai. BEVFormer: Learning bird’s-eye-view representation from multi-camera images via spatiotemporal transformers. In *ECCV*, 2022. 1, 2, 6
- [21] Tsung-Yi Lin, Piotr Dollár, Ross Girshick, Kaiming He, Bharath Hariharan, and Serge Belongie. Feature pyramid networks for object detection. In *CVPR*, 2017. 2, 6, 11
- [22] Tsung-Yi Lin, Priya Goyal, Ross Girshick, Kaiming He, and Piotr Dollár. Focal loss for dense object detection. In *ICCV*, 2017. 2, 5, 11
- [23] Shu Liu, Lu Qi, Haifang Qin, Jianping Shi, and Jiaya Jia. Path aggregation network for instance segmentation. In *CVPR*, 2018. 11
- [24] Yingfei Liu, Tiancai Wang, Xiangyu Zhang, and Jian Sun. PETR: Position embedding transformation for multi-view 3d object detection. In *ECCV*, 2022. 1, 3, 5, 6, 7
- [25] Ilya Loshchilov and Frank Hutter. SGDR: stochastic gradient descent with warm restarts. In *ICLR*, 2017. 5
- [26] Ilya Loshchilov and Frank Hutter. Decoupled weight decay regularization. In *ICLR*, 2019. 5
- [27] Arsalan Mousavian, Dragomir Anguelov, John Flynn, and Jana Kosecka. 3d bounding box estimation using deep learning and geometry. In *CVPR*, 2017. 1
- [28] Dennis Park, Rares Ambrus, Vitor Guizilini, Jie Li, and Adrien Gaidon. Is pseudo-lidar needed for monocular 3d object detection? In *ICCV*, 2021. 2, 5, 6
- [29] Jonah Philion and Sanja Fidler. Lift, splat, shoot: Encoding images from arbitrary camera rigs by implicitly unprojecting to 3d. In *ECCV*, 2020. 2
- [30] Joseph Redmon, Santosh Divvala, Ross Girshick, and Ali Farhadi. You only look once: Unified, real-time object detection. In *CVPR*, 2016. 2
- [31] Shaoqing Ren, Kaiming He, Ross Girshick, and Jian Sun. Faster R-CNN: Towards real-time object detection with region proposal networks. In *NeurIPS*, 2015. 2, 3, 5, 11
- [32] Danila Rukhovich, Anna Vorontsova, and Anton Konushin. Imvoxelnet: Image to voxels projection for monocular and multi-view general-purpose 3d object detection. In *WACV*, 2022. 1, 2
- [33] Andrea Simonelli, Samuel Rota Bulò, Lorenzo Porzi, Manuel Lopez-Antequera, and Peter Kontschieder. Disentangling monocular 3d object detection. In *ICCV*, 2019. 1, 2
- [34] Zhi Tian, Chunhua Shen, Hao Chen, and Tong He. FCOS: Fully convolutional one-stage object detection. In *ICCV*, 2019. 2
- [35] Ashish Vaswani, Noam Shazeer, Niki Parmar, Jakob Uszkoreit, Llion Jones, Aidan N Gomez, Łukasz Kaiser, and Illia Polosukhin. Attention is all you need. In *NeurIPS*, 2017. 3
- [36] Chien-Yao Wang, Hong-Yuan Mark Liao, Yueh-Hua Wu, Ping-Yang Chen, Jun-Wei Hsieh, and I-Hau Yeh. Cspnet: A new backbone that can enhance learning capability of CNN. In *CVPR Workshops*, 2020. 11

- [37] Tai Wang, Xinge Zhu, Jiangmiao Pang, and Dahua Lin. FCOS3D: fully convolutional one-stage monocular 3d object detection. In *ICCVW*, 2021. 1, 2, 6
- [38] Tai Wang, Xinge Zhu, Jiangmiao Pang, and Dahua Lin. Probabilistic and geometric depth: Detecting objects in perspective. In *CoRL*, 2021. 1, 2, 6
- [39] Yue Wang, Vitor Guizilini, Tianyuan Zhang, Yilun Wang, Hang Zhao, and Justin Solomon. DETR3D: 3d object detection from multi-view images via 3d-to-2d queries. In *CoRL*, 2021. 1, 3, 5, 6
- [40] Enze Xie, Zhiding Yu, Daquan Zhou, Jonah Philion, Anima Anandkumar, Sanja Fidler, Ping Luo, and Jose M Alvarez. M²BEV: Multi-camera joint 3d detection and segmentation with unified birds-eye view representation. *arXiv preprint arXiv:2204.05088*, 2022. 5, 6
- [41] Brady Zhou and Philipp Krähenbühl. Cross-view transformers for real-time map-view semantic segmentation. In *CVPR*, 2022. 3
- [42] Xingyi Zhou, Dequan Wang, and Philipp Krähenbühl. Objects as points. *CoRR*, abs/1904.07850, 2019. 1
- [43] Benjin Zhu, Zhengkai Jiang, Xiangxin Zhou, Zeming Li, and Gang Yu. Class-balanced grouping and sampling for point cloud 3d object detection. *arXiv preprint arXiv:1908.09492*, 2019. 5
- [44] Xizhou Zhu, Weijie Su, Lewei Lu, Bin Li, Xiaogang Wang, and Jifeng Dai. Deformable DETR: deformable transformers for end-to-end object detection. In *ICLR*, 2021. 2

A. Experiments with More Architectures

We provide more experiments with different 2D detectors and feature extractors in this section. The 2D detector part of MV2D is pretrained on nuImages [2], then the 2D detector part and 3D detector part are jointly trained on nuScenes *train* set. 3D object detection performance and model latency are evaluated on nuScenes *val* set [2]. For model latency, we only consider the latency of the network forward pass and ignore the pre-processing and post-processing time (e.g., image loading). The latency is evaluated on a single NVIDIA RTX 3090 GPU with batch size 1. We provide the detailed model architectures below.

A.1. Model Architecture

2D detector We choose 3 kinds of 2D detectors, including Faster R-CNN [31], a single-stage anchor-based 2D detector RetinaNet [22], and a single-stage anchor-free 2D detector YOLOX [8].

Feature extractor We choose 2 kinds of feature extractor, including ResNet-50 [13] with FPN [21] and CSPDarkNet-S [8, 36] with PAN [23]. ResNet-50 is equipped with deformable convolution [6] in the 3rd and 4th stages. CSPDarkNet-S with PAN is a lightweight feature extractor to validate the generalization ability of MV2D with small models. Moreover, the output channels of CSPDarkNet-S with PAN is 128, while that of ResNet-50 with FPN is 256.

Feature pyramid For models with CSPDarkNet-S backbone, the feature pyramid is built to produce feature maps with downsample stride {8, 16, 32}. For models with ResNet-50 backbone and Faster R-CNN detector, the feature pyramid is built to produce feature maps with downsample stride {4, 8, 16, 32, 64}. For models with ResNet-50 backbone and RetinaNet/YOLOX detector, the feature pyramid is built to produce feature maps with downsample stride {8, 16, 32, 64, 128}.

A.2. Latency and Performance Comparison

We equip MV2D with different 2D detectors and feature extractors, then evaluate their latency and performance on nuScenes *val* set. The results are listed in Table 5 and Table 6. Both models use an input resolution of 1408×512 . **Feat Latency** includes the latency of backbone and neck (feature pyramid). **2D Det Latency** includes the latency of 2D detection part (e.g., RPN [9] and R-CNN [10]). **Head Latency** includes the latency of RoI-align [11], dynamic query generator and decoder.

As demonstrated in the results, MV2D with CSPDarkNet-S has lower latency compared to ResNet-50. Specifically, when using YOLOX as 2D detector, MV2D with CSPDarkNet-S has overall latency of 60ms (16.6

FPS), while achieving 32.2% mAP and 35.9% NDS. When replacing YOLOX with a stronger 2D detector Faster R-CNN, the **2D Det Latency** increases by about 14ms, and performance also improves by 1.9% and 1.7% on mAP and NDS respectively. The difference in **Head Latency** is mainly caused by the number of 2D proposals generated by different 2D detectors. As for MV2D with ResNet-50 backbone, we implement 3 kinds of 2D detectors and compare their performances. Among these 2D detectors, Faster R-CNN achieves higher mAP and NDS with a higher overall latency of 168ms (5.9 FPS). These experiments show that MV2D can generalize well to other feature extractors and 2D detectors.

Feat Extractor	2D Detector	Resolution	Feat Latency	2D Det Latency	Head Latency	Latency ↓	FPS↑
CSPDarkNet-S	YOLOX	1408×512	22ms	10ms	28ms	60ms	16.6
CSPDarkNet-S	Faster R-CNN	1408×512	22ms	24ms	31ms	77ms	12.9
Res-50	YOLOX	1408×512	73ms	22ms	31ms	126ms	7.9
Res-50	RetinaNet	1408×512	73ms	50ms	38ms	161ms	6.2
Res-50	Faster R-CNN	1408×512	86ms	48ms	34ms	168ms	5.9

Table 5. Latency comparison on nuScenes *val* set.

Feat Extractor	2D Detector	Resolution	mAP ↑	NDS↑	mATE	mASE	mAOE	mAVE	mAAE
CSPDarkNet-S	YOLOX	1408×512	0.322	0.359	0.745	0.272	0.700	1.213	0.302
CSPDarkNet-S	Faster R-CNN	1408×512	0.341	0.376	0.738	0.276	0.662	1.199	0.266
Res-50	YOLOX	1408×512	0.372	0.412	0.689	0.269	0.578	1.008	0.206
Res-50	RetinaNet	1408×512	0.376	0.413	0.711	0.276	0.544	1.084	0.229
Res-50	Faster R-CNN	1408×512	0.388	0.433	0.697	0.271	0.479	0.952	0.208

Table 6. Performance comparison on nuScenes *val* set.